International Journal of Engineering Research & Technology (IJERT)
ISSN: 2278-0181
Vol. 4 Issue 07, July-2015

Structure and Magnetic Properties of Lanthanum Strontium Ferrites Nanopowders Synthesized by Thermal Decomposition of Mixed Metal Acetyl Acetonates

E. A. Nforna
Lanochee
Department of Chemistry,
University of Dschang,
Cameroon,

J. N. Ghogomu
Lanochee
Department of Chemistry,
University of Dschang,
Cameroon,

P. A. Joy
Mmu, Pmcd,
CSIR-National Chemical Laboratory,
Pune 411008,
India

J. N. Lambi
Lmc
Department of Chemistry,
ENS Yaoundé,
University of Yaoundé I,
Cameroon

***Abstract*— Single phased, polycrystalline mixed metal oxides, $La_{1-x}Sr_xFeO_{3-\delta}$ (x = 0.0, 0.2, 0.3, 0.5) have been prepared via the thermal decomposition of mixed metal acetylacetonate precursors. The precursors were synthesized at 55 °C by coprecipitation and decomposed at 450 ºC to give multi-phased lanthanum strontium ferrite nanoparticles which were further calcined at 1000 ºC to obtain the single-phased perovskite ferrites. The decomposition temperature of the precursors was determined by thermogravimetric analysis (TGA). The perovskite ferrites were then characterized by X-ray diffraction (XRD), scanning electron microscopy (SEM) and energy dispersive spectroscopy (EDS). SEM and XRD analyses showed that the particles of the ferrites were spherical and nano-sized with structures ranging from orthorhombic to rhombohedral as the Sr content increased. For x = 0.0, 0.2, and 0.3 (orthorhombic), the average Fe–O bond length and the unit cell volume decreased with increasing Sr content.**

Magnetic properties were investigated at room temperature (27 °C) using a vibrating sample magnetometer and the hysteresis loops showed that all the compositions exhibit anti-ferromagnetic ordering with a weak ferromagnetic interaction related to their structures. Increasing coercive fields were also observed with increasing Sr content.

***Keywords*— $La_{1-x}Sr_xFeO_{3-\delta}$; acetylacetonate; co-precipitation; X-ray diffraction; ferromagnetic; anti-ferromagnetic.**

I. INTRODUCTION

A variety of materials of extreme importance to modern technology have ABO_3 structures. The most important being the perovskite-type materials which present structural compositions with ferroelectric properties and with high dielectric constants. Their immense interest or wide applications are ascribed to their tunable shapes. Substitution in the A or B-site of the ABO_3 perovskite structure modifies the properties of the perovskite material for specific areas of applications [1]. Lanthanum strontium ferrites, $La_{1-x}Sr_xFeO_3$, have recently been the focus of major research due to their applications in solid oxide fuel cells as cathode materials [2, 3, 4], in gas sensors [5], in catalysis [6] and in magnetic data storage, logic, sensors [7, 8, 9]. These applications have been attributed to the unique structural features of the rare earth ferrite perovskites [9, 10].

Rare earth ferrites with general formula, $ReFeO_3$ (where Re represents a rare earth element), have a tilted orthorhombic perovskite structure with unit cell dimensions a, b and c such that c is usually twice the length of either a or b. The cation sites are highly substitutable, thus modifying the structure and physical properties of the perovskite [10]. This may lead to new properties such as ferro-electric/magnetic, conductivity, piezoelectric, pyroelectric or magneto-optic properties for specific applications [1, 11, 12]. $LaFeO_3$ is a perovskite material where the unit cell consists of six O^{2-} ions around Fe^{3+} ions in an octahedral coordination. The La^{3+} ions enter the interstitial sites of the FeO_6 octahedron [13, 14]. Deviating from the ideal cubic perovskite, $LaFeO_3$ shows an orthorhombic setting with magnetic spins pointing along the a-axis and an anti-ferromagnetic component parallel to the a-axis. There is a weak ferromagnetic component caused by a slight canting (0.5º) of the antiparallel spins towards the c-axis [13, 14]. The magnetic properties of $LaFeO_3$ is due to Fe^{3+} ions and there is no magnetic interaction between Fe^{3+} and La^{3+} since La^{3+} is non-magnetic. Substituting Sr^{2+} for La^{3+} in ($La_{1-x}Sr_xFeO_{3-\delta}$) shows extensive modification of the structure and interesting magnetic, electronic and catalytic properties

[15]. The solid solution $La_{1-x}Sr_xFeO_{3-\delta}$ shows an orthorhombic structure from x=0.0 to x=0.2; mixed orthorhombic - rhombohedral at x=0.3; rhombohedral from x=0.4 to 0.5 [13].

Synthetic techniques strongly influence the structure and particle size of perovskites. Lanthanum strontium ferrite has been prepared by a variety of synthesis techniques such as solid state reaction method [16, 17], sol–gel [7], precipitation [18], combustion [11], polymeric method [14], etc. However, there are some disadvantages associated with these synthetic methods such as high temperatures [16, 17], long reaction time or slow diffusion [16, 19], formation of secondary or impurity phases [1] etc.

In this study, a circumvention or mitigation of the problems enumerated above is proposed wherein nanosized lanthanum strontium ferrites [$La_{1-x}Sr_xFeO_{3-\delta}$; x = 0, 0.2, 0.3, 0.5] have been prepared under atmospheric conditions by thermal decomposition or pyrolysis of the mixed metal acetylacetonates at a relatively low temperature of 450 ºC. Secondary phases that appeared at the decomposition temperature were eliminated after calcination at 1000 ºC for 6 hours. The advantages of this technique include: the use of metal acetylacetonates as single source precursors which are easy to prepare in solution at low temperatures, their stablility in air, their decomposition at relatively low temperatures to form the metal oxides and the fact that mixing of the metal ions in solution at the molecular level is homogenous thus ensuring the desired stoichiometry in the final product [20, 21]. The synthesized powders are then characterized by different spectroscopic methods.

II. EXPERIMENTAL

The following reagents of analytical grade were used: $C_5H_8O_2$ (99.5%, BDH); $La(NO_3)_3.6H_2O$ (99%), $Sr(NO_3)_2$ (99%), $Fe(NO_3)_3.9H_2O$ (99.5%), $Co(NO_3)_2.6H_2O$ (99%), and NaOH (98%) (Sigma-Aldrich),

The different perovskite nanopowders were prepared according to the formula $La_{1-x}Sr_xFeO_{3-\delta}$: {x=0.0 (LFO), 0.2 (LSF82), 0.3 (LSF73), 0.5 (LSF55)}, and the non stiochiometric $La_{0.7}Sr_{0.3}Fe_{1.05}O_{3-\delta}$ (LSF7305 - 5 % excess Fe) and $La_{0.7}Sr_{0.3}Fe_{1.1}O_{3-\delta}$ (LSF7310 - 10 % excess Fe) from the corresponding mixed metal acetylacetonate precursors by thermal decomposition [20, 22, 23].

The mixed metal acetylacetonate precursors were prepared by co-precipitation [24, 25]. $La_{0.7}Sr_{0.3}Fe(C_5H_7O_2)_6$ (x=0.3, LSF73acac) was prepared as follows: Sodium acetylacetonate, a precipitating agent, was first prepared by adding dropwise stoichiometric amount of 3 ml (2.916 g) acetylacetone (acacH) to a solution of NaOH (2.4 M) maintained at 50 ºC while stirring on a magnetic stirrer for 20 minutes.

1.47 g of $La(NO_3)_3.6H_2O$, 0.309 g of $Sr(NO_3)_2$ and 1.959 g of $Fe(NO_3)_3.9H_2O$ were dissolved in 10 ml double distilled water and slowly added to the hot solution of sodium acetylacetonate while stirring for 30 minutes. Red precipitate of $La_{0.7}Sr_{0.3}Fe(C_5H_7O_2)_6$ was formed. The precipitate was allowed to cool, filtered by suction, washed three to four times with distilled water to remove by-products and unreacted reactants and dried for 5 hours at 80ºC in a dessicator. The yield was 92.7%.

The synthesis of $LaFe(C_5H_7O_2)_6$ (LFOacac), $La_{1-x}Sr_xFe(C_5H_7O_2)_6$ {x=0.2 (LSF82acac), 0.5 (LSF55acac)} and the non stoichiometric $La_{0.7}Sr_{0.3}Fe_{1.05}(C_5H_7O_2)_6$ (LSF7305acac) and $La_{0.7}Sr_{0.3}Fe_{1.1}(C_5H_7O_2)_6$ (LSF7310acac) was each carried out by the same procedure.

The mixed metal oxides were formed by thermal decomposition of the mixed metal acetylacetonate complexes by putting into a preheated muffle furnace at 450 ºC in air for three hours. The powders formed were ground and calcined at 1000 ºC for 6 hours at a heating and cooling rate of 5 ºC/min.

Thermogravimetric studies of one of the acetylacetonate precursors – LSF73acac was carried out using a TG analyser (Model: SDT Q600 V20.9 Build 20 DSC-TGA Standard) in air, at a heating rate of 10 °C/min in an alumina crucible. The temperature range was between room temperature and 900 °C. For each composition calcined at 1000 ºC, phase purity and crystal structure were determined by powder X-ray diffraction (PANalytical X'Pert PRO 1712) in the 2θ range of 10-80º, using Cu-Kα radiation. The structural refinements were carried out with the Rietveld method of profile analysis using GSAS. Crystallite size was determined based on Scherer's formula from the line broadening of the peak at around 32°. The morphology of the powders calcined at 1000 ºC was examined using a JEOL JSM-840A scanning electron microscope fitted with an energy dispersive X-ray spectrometer (EDS). The magnetization measurements were performed using a vibrating sample magnetometer, VSM (model EG&G PAR 4500) at room temperature (300 K) with applied field from 0 to 15 KOe.

III. RESULTS AND DISCUSSION

A. TGA and DTA

It is vital to study the thermal decomposition chemistry of the acetylacetonate precursors as it indicates the total weight loss on heating, the formation of intermediate phases, and the temperature at which all the organic fraction is removed and final product formed.

The TGA and DTA curves of one of the precursors, LSF73acac is presented in fig. 1. The DTA curve indicates four important temperature points namely: 74.02, 172.9, 454.5 and 617.9 °C respectively. The first weight loss of 3.8 % occurred in the temperature range 70.4 -140.4 ºC and is probably due to the partial vaporization of the compound. Acetylacetonates sublime at low temperatures [24]. The second weight loss of 65.3 % occurred in the temperature range 148.3 – 230.9 ºC and is attributed to the decomposition of the acetyacetonate group as six molecules of acetone (theoretical 57.6%) and CO_2 (theoretical 5.7%). The third weight loss of 7.9 % occurred in the temperature range 352.1 - 500 ºC and is attributed to the decomposition of secondary phases like $La_2(CO_3)_2$ to release CO_2 (5.7%). %). Lanthanum oxycarbonate was obtained at 550 ºC as intermediate by [26] during the thermal decomposition of lanthanum metalorganics.The fourth weight loss of 2.6 % occurred between 613 – 648.7 ºC and is attributable to the removal of H_2O (theoretical 2.3%) from a secondary phase such as $La_2O_2(OH)_2$. XRD patterns were recorded for the resulting powders formed at different decomposition temperatures (between 400 - 1000 °C) and indicated the presence of lanthanum oxy-hydroxy carbonates at temperatures less than 800 °C.

With about 3% of the compound lost by sublimation, the percentage residue was equal to 20.2% (theoretical 21.1%) and corresponds to $La_{0.7}Sr_{0.3}FeO_3$. Fe_2O_3 was obtained as residue by [23] from the decomposition of iron(III) acetylacetonate.On their own part, [27] observed the evolution of acetone and CO_2 from the decomposition of iron(III) acetylacetonate.

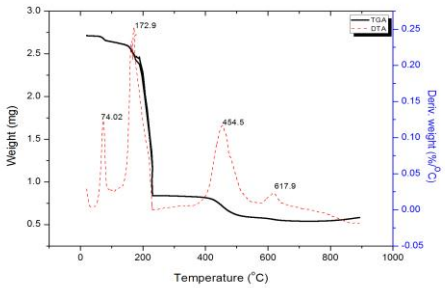

Fig. 1. *TGA and DTA curves for* LSF73acac

B. Synthesis of nanopowders

Lanthanum ferrite ($LaFeO_3$) and lanthanum strontium ferrite ($La_{1-x}Sr_xFeO_{3-\delta}$) were synthesized from the acetylacetonate precursors by thermal decomposition. Various synthetic parameters such as decomposition temperature of the precursors, calcination temperature and time for the formation of single phase were investigated. Process optimization was carried out on the composition $La_{0.7}Sr_{0.3}FeO_{3-\delta}$. Decomposition temperature of each metal acetylacetonate is less than 450 °C [24, 27]. Based on the optimization conditions, the TGA/DTA curves and the fact that the decomposition temperature of each of the metal acetylacetonates is less than 450 °C [24, 27], thermal decomposition of the metal acetylacetonate precursors was carried out at 450 °C to ensure rapid decomposition of all the components in the mixture at the same time to form the desired perovskite phase. The small amounts of secondary phases formed at 450 °C merged to a single phase after calcination at 1000 °C for 6 hours. All characterizations were carried out on the $La_{1-x}Sr_xFeO_{3-\delta}$ polycrystalline powders obtained at 1000 °C.

C. Structure and particle size (XRD)

The XRD patterns of all the compositions of $La_{1-x}Sr_xFeO_{3-\delta}$ obtained at 1000 °C are presented in fig. 2.

The grain sizes were calculated at $2\theta = 32$ (most intense peak) according to the Scherrer formula:

$$D = K\lambda / \beta\cos\theta \qquad (1)$$

Where *K* is a constant, its value 0.9 for spherical particles, λ is the x-ray wavelength, θ is the Bragg's angle and β is the full width at half maxima at reflecting intensity peaks. All the compositions showed particle sizes less than 100 nm (table 1).

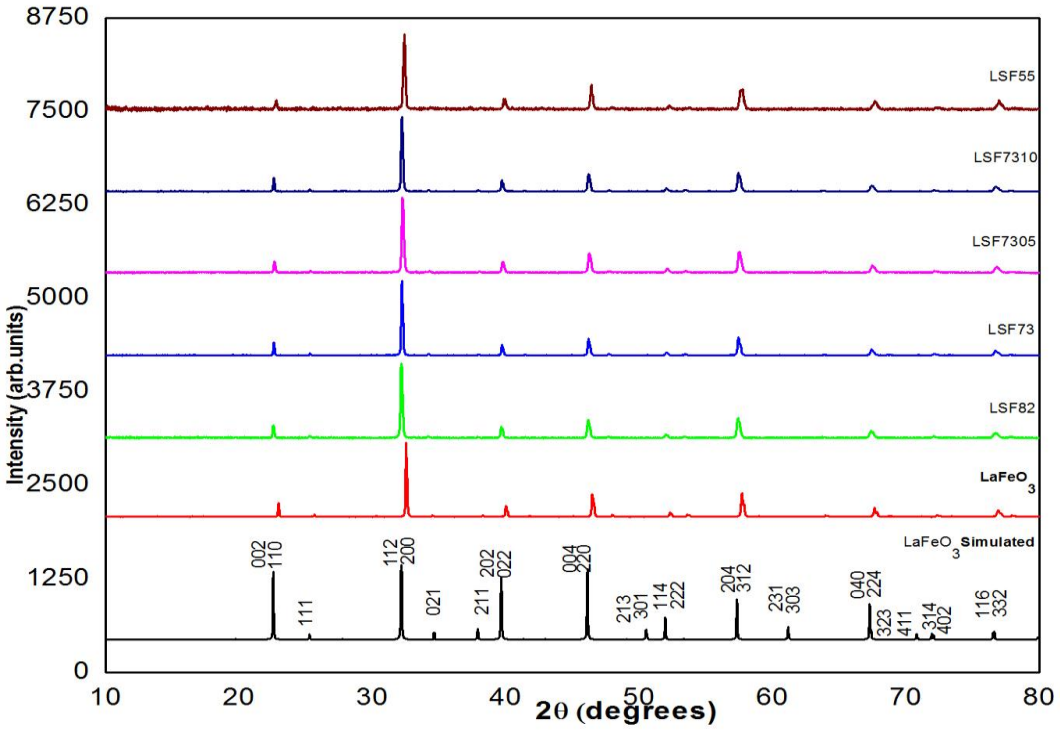

Fig. 2. XRD pattern of $LaFeO_3$ simulated, LFO, LSF82, LSF73, LSF7305, LSF7310 and LSF55

TABLE I. PARTICLE SIZES OF $La_{1-x}Sr_xFeO_{3-\delta}$ AND THE NON STIOCHIOMETRIC COMPOSITION

Sample	LFO	LSF82	LSF73	LSF7305	LSF7310	LSF55
	X=0 $LaFeO_3$	X=0.2 ($La_{0.8}Sr_{0.2}FeO_{3-\delta}$)	X=0.3 ($La_{0.7}Sr_{0.3}FeO_{3-\delta}$)	X=0.3 ($La_{0.7}Sr_{0.3}Fe_{1.05}O_{3-\delta}$)	X=0.3 ($La_{0.7}Sr_{0.3}Fe_{1.1}O_{3-\delta}$	X=0.5 ($La_{0.5}Sr_{0.5}FeO_{3-\delta}$
Mean grain size (nm)	61	48	56	45	51	40

The XRD patterns of the solid solution, $La_{1-x}Sr_xFeO_{3-\delta}$ all show the formation of a single phase perovskite. From the diffraction pattern, the unsubstituted lanthanum ferrite, LFO (x=0.0) shows an orthorhombic structure, with space group Pbnm (62) according to JCPDS file Nº 74-2203, in agreement with results previously reported [1, 11]. LSF82 (x=0.2), the stoichiometric composition LSF73 (x=0.3), and the non stoichiometric compositions LSF7305 and LSF7310 (x=0.3) show single phase orthorhombic structures as indexed in JCPDS No 35-1480 [1, 11, 18]. The composition $La_{0.5}Sr_{0.5}FeO_{3-\delta}$ (x=0.5, LSF55) shows a rhombohedral structure as indexed in JCPDS No 82-1962, with space group R-3c (167). Increasing Sr^{2+} substitution for La^{3+} changes the structure from orthorhombic to rhombohedral. Lattice parameters and some selected bond lengths and angles from Rietveld refinement of the orthorhombic perovskite phases ($La_{1-x}Sr_xFeO_{3-\delta}$ x=0.0, 0.2, 0.3), with space group Pbnm, is summarized in table 2. The observed and calculated XRD patterns of the typical refined XRD patterns of LaFeO3 is given in fig. 3. There is good agreement between the observed and calculated patterns. From table 2, increasing Sr^{2+} substitution results in decrease of the unit cell volume from 242·30 - 241.511 Å for the orthorhombic structures. There is abrupt increase in unit cell volume for the rhombohedral structure, x=0.5 according to the literature (JCPDS Nº 82-1962).

Although the ionic radius of Sr^{2+} (118 pm) is larger than that of La^{3+} (116 pm) [28] the replacement of La^{3+} by Sr^{2+} results in a contraction of unit cell volume which is explained hereafter. Sr^{2+} substitution for La^{3+} results in the formation of Fe^{4+} ions to maintain electrical neutrality. The Fe^{4+} ions are smaller than Fe^{3+}. The smaller Fe^{4+} ions strengthen the Fe–O bond in the FeO_6 octahedra according to Pauling's rule [29] leading to increased covalency and shorter bond length. These effects are stronger than the effect of the substitution of the large Sr^{2+} ions. Hence, there is contraction of unit cell volume for low Sr substitutions (x=0.1- 0.3), similar to other results reported [4, 7, 18, 30]. As the Sr content increases, formation of oxygen vacancies dominates the formation of Fe^{4+}. The unit cell volume increases due to the substitution of the larger Sr^{2+} ions as observed for x=0.5 [30]. Even increasing the amount of Fe by up to 10% in excess still forms monophase perovskite.

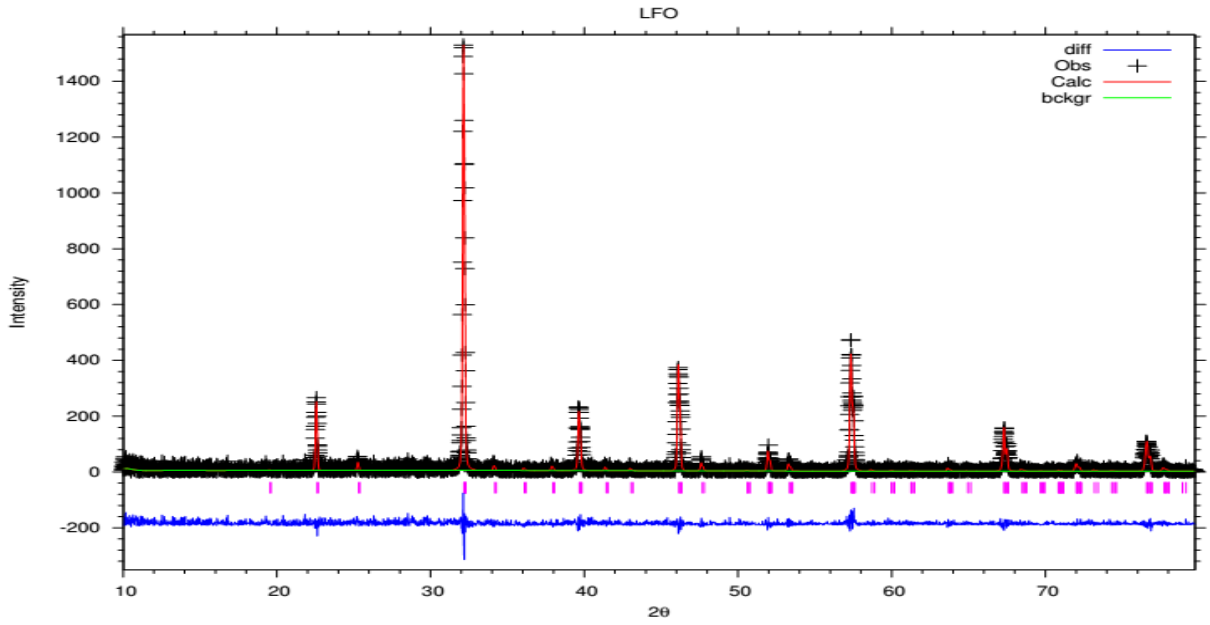

Fig. 3. Observed (cross) and calculated (continuous line) intensities in the XRD pattern of LFO. The differences between observed and calculated intensities are plotted at the botto

TABLE II. RIETVELD REFINED STRUCTURAL PARAMETERS FOR $La_{1-x}Sr_xFeO_{3-\delta}$ x=0.0, 0.2, 0.3 – LITERATURE VALUES (JCPDS) IN PARENTHESES

Compounds Literature - JCPDS Nº	$LaFeO_3$ [74-2203]	$La_{0.8}Sr_{0.2}FeO_{3-\delta}$ [35-1480]	$La_{0.7}Sr_{0.3}FeO_{3-\delta}$	$La_{0.5}Sr_{0.5}FeO_{3-\delta}$ [82-1962]
Crystal system		Orthorhombic		Rhombohedral
Space group		Pbnm (62)		
Lattice				parameters
a (Å)	5·5522(7)	5.5506(10)	5.55157(19)	
	[5.553]	[5.532]		[5.511]
b (Å)	5·5597(4)	5.5516(7)	5.54860(19)	
	[5.563]	[5.553]		[5.511]
c (Å)	7·8494(6)	7.8444(14)	7.84037(26)	
	[7.867]	[7.835]		[13.416]
Cell volume ($Å^3$)	242·30(4)	241.73(7)	241.511(14)	
	[243.02]	[240.68]		[352.87]
Bond lengths (Å)				
Fe–O1	1.99319(14)	1.97001(34)	1.94957(5)	
Fe–O2′	1.95106(13)	1.96772(22)	2.02487(6)	
Fe–O2″	2.08045(18)	2.03273(22)	2.02553(5)	
Bond angles (°)				
Fe–O1–Fe	159.811(3)	169.097(3)	150.938(1)	
Fe–O2–Fe	154.042(1)	157.741(4)	161.694(0)	

D. Microstructure and morphology (SEM)

The SEM micrographs of LFO, LSF82, LSF73, LSF7305, LSF7310 and LSF55 calcined at 1000 ºC are shown in fig. 4. The micrographs show spherical particles with grain sizes less than 100 nm in agreement with XRD results. The particles have a great tendency of agglomeration in agreement with results previously reported [11, 31]. These SEM images also reveal that the powders show homogeneity in form and compositions.

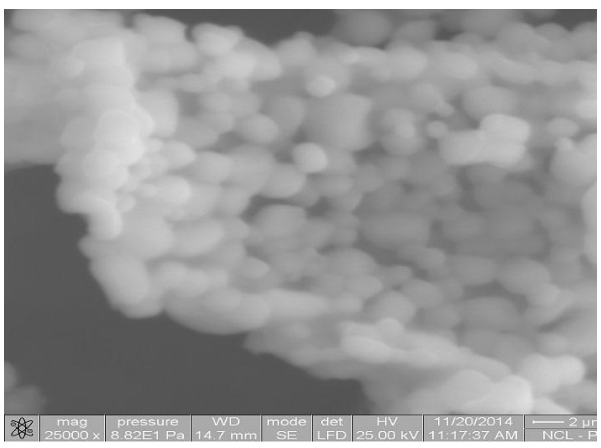

(a)

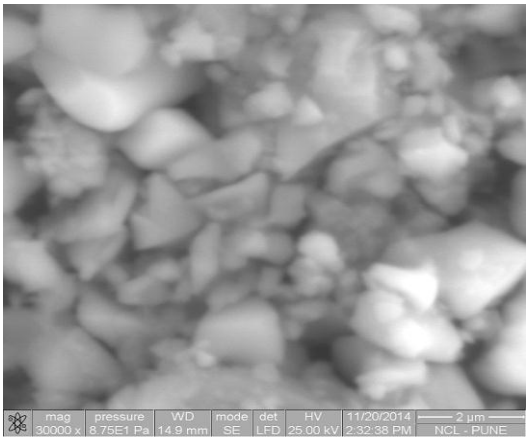

(b)

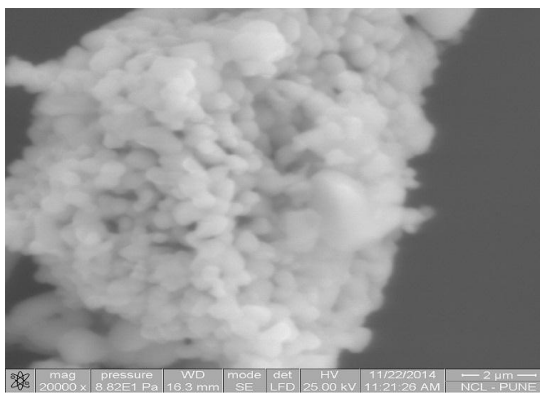

(c)

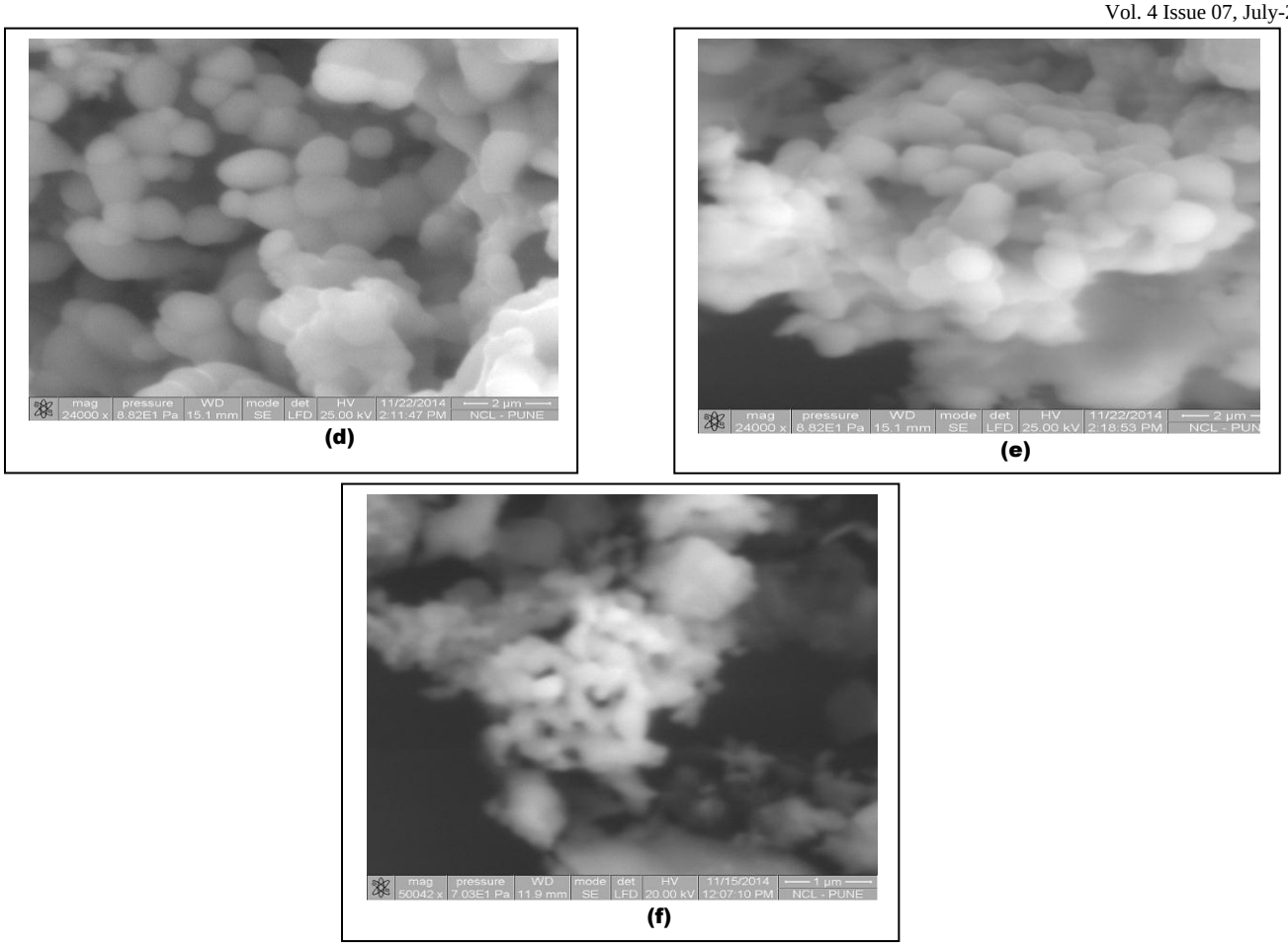

Fig. 4. SEM micrographs of (a) LFO, (b) LSF82, (c) LSF73, (d) LSF7305, (e)LSF7310 at 2 µm and (f) LSF55 at 1 µm

Elemental analysis (EDS)

Table 3 summarizes the elemental weight percentages in each composition from EDS. The experimental metal ratios are better compared with theoretical values by calculating (La+Sr):Fe ratios rather than the single metal ratios since EDS is a surface technique which focuses on small regions of the sample. The experimental metal ratios are presented thus: LFO – La:Fe is 1:1; LSF82 – (La,Sr):Fe is 0.9:1; LSF73 – (La,Sr):Fe is 1.1:1; LSF7305 – (La,Sr):Fe is 1:1.05; LSF7310 – (La,Sr):Fe is 1.1:1.1; LSF55 – (La,Sr):Fe is 1:1. The metal-metal ratios, within acceptable error limits, are therefore close to the expected stoichiometric values (theoretical La+Sr:Fe – 1:1). No other elements were detected.

TABLE III. ELEMENTAL ANALYSIS OF LFO, LSF82, LSF73, LSF7305, LSF7310 AND LSF55 FROM EDS

Compound	LFO	LSF82	LSF73	LSF7305	LSF7310	LSF55
Element	Weight % (theoretical)	Weight % (theoretical)	Weight % (theoretical)	Weight % (theoretical)	Weight % (theoretical)	Weight % (theoretical)
La	52.29 (57.2)	49.20 (47.8)	49.45 (42.7)	49.02 (42.3)	45.97 (41.8)	38.67 (32)
Sr		4.46 (7.5)	9.69 (11.5)	8.07 (11.4)	10.68 (11.3)	13.07 (20.2)
Fe	21.79 (23)	22.95 (24)	21.78 (24.5)	24.88 (25.5)	22.86 (26.4)	23.41 (25.7)
O	25.92 (19.8)	23.39 (20.6)	19.07 (21.1)	18.03 (20.9)	20.49 (20.6)	24.84 (22.1)
Total	100	100	100	100	100	100

E. Magnetic measurements

Magnetic measurements were performed on the $La_{1-x}Sr_xFeO_{3-\delta}$ nanopowders obtained after calcination at 1000 °C with a maximum applied magnetic field of 15 kOe. Fig. 5 presents the hysteresis loops measured at 27 °C and table 4 shows the coercive force and magnetization at maximum applied field. We observe spontaneous magnetization and the appearance of hysteresis loops at room temperature (fig.5). The maximum field applied, 15 kOe does not saturate the magnetization. We also note a closed loop at the maximum applied field. The shape of the hysteresis loops indicates weak ferromagnetism and the non-saturation of the magnetization is characteristic of anti ferromagnetic ordering of the spins in the nanoparticles. Other researchers have reported similar results [7, 14, 32]. The magnetization increases with Sr content. Majunath B. And Manivannan, 2010 [33] observed increased magnetization with increased K substitution for La in lanthanum ferrite. Increasing Sr substitution (up to x=0.3) increases the coercive force while there is a little decrease when x=0.5. These observations can be understood from structural variation. $LaFeO_3$ is a G-type spin ordered anti ferromagnetic orthoferrite [34]. The magnetic moments of two neighbouring Fe^{3+} ions are coupled through the O^{2-} ions between the Fe^{3+}–O–Fe^{3+} known as super-exchange interactions in anti ferromagnetic spin order along the a-axis [7, 14, 35]. The spin canting resulting from the tilted FeO_6 octahedra gives rise to a weak ferromagnetism along the c-axis. With increasing Sr substitution, the Fe–O bond reduces and the introduction of large Sr^{2+} cations decreases the tilts of the octahedra which strengthen the antiferromagnetic super-exchange ordering. Formation of Fe^{4+} ions resulting from the substitution of Sr^{2+} for La^{3+} leads to Fe^{4+}–O–Fe^{3+} interaction called double exchange interaction. This interaction strengthens the ferromagnetic component [7] and the presence of oxygen vacancies can also disturb the super-exchange interactions, increasing the ferromagnetism. From structural considerations, for low Sr substitutions, the double exchange interaction is significant and when x=0.5, oxygen vacancies are more important. It was similarly observed as reported by [7] that for nanoparticles, magnetic moments due to uncompensated surface spins contribute to the increase of magnetization.

TABLE IV. COERCIVE FORCE OF $La_{1-x}Sr_xFeO_{3-\delta}$ AND THE NON STOICHIOMETRIC COMPOSITIONS.

Compound	LFO	LSF82	LSF73	LSF7305	LSF7310	LSF55
Coercive force (Oe)	356.4	621.6	1255	1209.7	998.5	920.1
Magnetization at maximum applied field (emu/g)	0.16	1.06	1.5	1.53	2.4	5.66

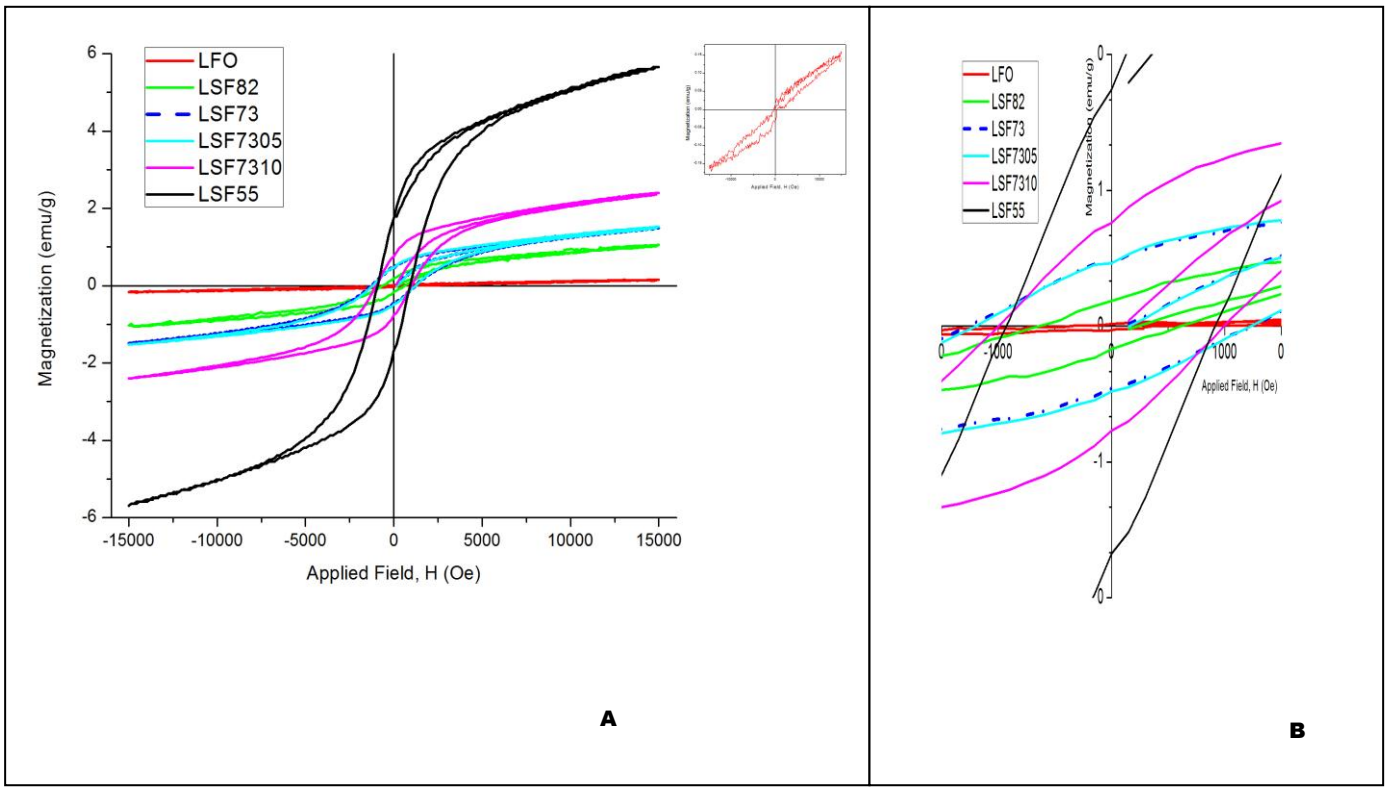

Fig. 5. Hysteresis loops of (A) LFO, LSF82, LSF73, LSF7305, LSF7310 and LSF55 and LFO in the inset at room temperature (B) enlarged loops to show variation of coercive fields.

IV. CONCLUSION

The solid solution with formula $La_{1-x}Sr_xFeO_{3-\delta}$ (x=0, 0.2, 0.3, 0.5) were synthesized by metal organic decomposition of the mixed metal acetylacetonate complexes. XRD patterns showed monophasic orthorhombic to rhombohedral structures with increasing Sr content and contraction of the lattice for the orthorhombic compositions. There is spontaneous magnetization of all compositions when an external magnetic field is applied. All samples exhibit a hysteresis loop characterized by coexisting anti ferromagnetic and weak ferromagnetic interactions. Sr substitution increases the coercive force. These compounds have potential magnetic applications in data storage, logic, magnetic storage etc.

ACKNOWLEDGEMENTS

This work was partly financed by the Government of India through FICCI under the "C V Raman International Fellowship for African Researchers" program to E. A. Nforna. Special thanks equally go to the University of Dschang (Cameroon) for research grants to meritorious postgraduate students which helped a great deal towards the completion of this research project.

REFERENCES

[1] U.F. Vogt, J. Sfeir, J. Richter, C. Soltmann, and P. Holtappels, B-site substituted lanthanum strontium ferrites as electrode materials for electrochemical applications, Pure Appl. Chem., Vol. 80, No. 11 pp. 2543-2552, 2008.

[2] C.O. Augustin, R. Kalai, R. Nagaraj, L. J. Berchmans, Effect of La^{3+} substitution on trhe structural, electrical and electrochemical properties of strontium ferrite by citrate combustion method, Materials Chemistry and Physics, 89 pp. 406-411, 2005.

[3] M. Søgaard, P.V. Hendriksen, M. Mogensen, Oxygen nonstoichiometry and transport properties of strontium substituted lanthanum ferrite, Journal of Solid State Chemistry 180 pp. 1489 – 1503, 2007.

[4] M.V. Patrakeev, J.A. Bahteeva, E.B. Mitberg, I.A. Leonidov, V.L. Kozhevnikov and K.R. Poeppelmeier, Electron/hole and ion transport in $La_{1-x}Sr_xFeO_{3-\delta}$, Journal of Solid State Chemistry 172 pp. 219 – 231, 2003.

[5] H. Liu, H. Fan, X. Xu, H. Lu, T. Zhang, Synthesis and gas sensing characteristics of $La_xSr_{1-x}FeO_3$ nanofibers via electrospinning, Solid-State Electronics 79 pp. 87–91, 2013.

[6] A. Wattiaux, J. C. Grenier, M. Pouchard, and P. Hagenmuller, J. Electrochem. Soc. 134 pp. 1718, 1987.

[7] J. Li, X. Kou, Y. Qin, and H. He, Microstructure and magnetic properties of $La_{1-x}Sr_xFeO_3$ nanoparticles, Phys. stat. sol. , 191, No. 1 pp. 255–259, 2002.

[8] A.H. Bobeck, Properties and device applications of magnetic domains in orthoferrites, the Bell System Technical Journal, pp. 1901-1925, 1967.

[9] A. Goldman, Modern Ferrite Technology, second edition, Springer Science+Business Media, Inc., New York, 2006.

[10] D. W. Richerson, Modern ceramic Engineering: properties, processes and use in design, second edition, revised and expanded, Marcel Dekker, inc., New York, 1992, p. 288

[11] I. N. Sora, F. Fontana, R. Passalacqua, C. Ampelli, S. Perathoner, G. Centi, F. Parrino, L. Palmisano, Photoelectrochemical properties of doped lanthanum orthoferrites, Electrochimica Acta 109 pp. 710–715, 2013.

[12] J.R. Hayes and A.P. Grosvenor, An X-ray absorption spectroscopic study of the electronic structure and bonding of rare-earth orthoferrites, J. Phys.: Condens. Matter **23** pp. 465502 (8pp), 2011.

[13] R. B. Da Silva, J. H. Araújo, J. M. Soares, F. L. A. Machado, Maussbauer and Magnetic Characterization of the Nanocrystalline Perovskites $La_{1-x}Sr_xFeO_{3-\delta}$ ($0 \leq x \leq 0.5$), 11th International Conference on Advanced Materials Brazil, 2009.

[14] M. Popa, J.M.C. Moreno, Lanthanum ferrite ferromagnetic nanocrystallites by a polymeric precursor route, Journal of Alloys and Compounds, 509 pp. 4108–4116, 2011.

[15] J. Mizusaki, M. Yoshihiro, S. Yamauchi, and K. Fueki, Nonstoichiometry and defect structure of the perovskite-type oxides $La_{1-x}Sr_xFe0_{3-\delta}$, Journal of Solid State Chemistry, 58 pp. 257-266, 1985.

[16] A. Chainani, M. Mathew, and D. D. Sarma, Electronic structure of $La_{1-x}Sr_xFeO_3$, The American Physical Society, vol. 48, 14 pp. 818, 1993.

[17] J. Ma, J. Q. Yan, S. O. Diallo, R. Stevens, A. Llobet, F. Trouw, D. L. Abernathy, M. B. Stone, and R. J. McQueeney, Role of magnetic exchange energy on charge ordering in $R_{1/3}Sr_{2/3}FeO_3$ (R = La, Pr, and Nd), Physical Review B 84 pp. 224115, 2011.

[18] A. Evdou, V. Zaspalis, L. Nalbandian, $La_{1-x}Sr_xFe0_{3-\delta}$ perovskites as redox materials for application in a membrane reactor for simultaneous production of pure hydrogen and synthesis gas, Fuel 89 pp. 1265–1273, 2010.

[19] M. Sivakumar, A. Gedanken, W. Zhong, Y. H. Jiang, Y. W. Du, I. Brukental, D. Bhattacharya, Y. Yeshurun and I. Nowik, Sonochemical synthesis of nanocrystalline $LaFeO_3$, J. Mater. Chem., 14 pp. 764-769, 2004.

[20] R. W. Schwartz, T. Schneller, R. Waser, Chemical solution deposition of electronic oxide films, C. R. Chimie 7 pp. 433–461, 2004.

[21] C. M. Lieberman, A. Navulla, H. Zhang, A. S. Filatov, and E.V. Dikarev, Mixed-Ligand Approach to Design of Heterometallic Single-Source Precursors with Discrete Molecular Structure, Inorg. Chem., 53, 2014.

[22] H. Itoh, T. Takeda, S. Naka, Preparation of nickel and Ni-Zn ferrite films by thermal decomposition of metal acetylacetonates, Journal of Materials Science, 21 pp. 3677-3680, 1986 .

[23] B. Pal , M. Sharon, Preparation of iron oxide thin film by metal organic deposition from Fe III -acetylacetonate: a study of photocatalytic properties, Thin Solid Films 379, pp. 83-88, 2000.

[24] K. Binnemans, Handbook on the Physics and Chemistry of Rare Earths, Elsevier B. V., Vol. 35 DOI: 10.1016/S0168-1273 (05) pp. 35003-3, 2005.

[25] A.C. Jones, MOCVD of Electroceramic Oxides: A Precursor manufacturer's perspective, Chem. Vap. Deposition, 4, No. 5 pp. 169-179, 1998.

[26] L. Ciontea a, M. Nasui, T. Petrisor Jr., R.B. Mos, M.S. Gabor, R.A. Varga, T. Petrisor, Synthesis, crystal structure and thermal decompositio n of $[La_2(CH_3CH_2COO)_6.(H_2O)_3]$ $3.5H_2O$ precursor for high-k La_2O_3thin films deposition Materials Research Bulletin 45, pp 1203–1208, 2010.

[27] J.V. Hoene, R. G. Charles and W. M. Hickam, Thermal decomposition of metal acetylacetonates mass spectroscopy studies, 62, 440 pp 1098-1101, I958.

[28] Shriver and Atkins, Inorganic Chemistry, 5th edition, Oxford University Press, Great Britain, 2010, pp. 783-784.

[29] L. Pauling, The Nature of the Chemical Bond, 3rd edn., Cornell Univ. Press, Ithaca, NY, 1960.

[30] N. Dasgupta, R. Krishnamoorthy, K. T. Jacob, Crystal structure and thermal and electrical properties of the perovskite solid solution $Nd_{1-x}Sr_xFeO_{3-\delta}$ ($0 \leq x \leq 0.4$), Solid State Ionics 149 pp. 227– 236, 2002.

[31] D. Bayraktar, F. Clemens, S. Diethelm, T. Graule, J. V. Herle, P. Holtappels, Production and properties of substituted $LaFeO_3$-perovskite tubular membranes for partial oxidation of methane to syngas, Journal of the European Ceramic Society 27 pp. 2455–246, 2007.

[32] I. N. Sora, T. Caronna, F. Fontana, C. d. J. Fernandez, A. Caneschi, M. Green, Crystal structures and magnetic properties of strontium and copper doped lanthanum ferrites, Journal of Solid State Chemistry 191 pp. 33–39, 2012.

[33] M. B. Bellakki and V. Manivannan, Solution combustion synthesis of (La, K)FeO_3 orthoferrite ceramics: structural and magnetic property studies, Bull. Mater. Sci., Vol. 33, No.5 pp. 611–618, 2010.

[34] T. Peterlin-Neumaier and E. Steichele, Antiferromagnetic structure of $LaFeO_3$ from high resolution to neutron diffraction, J. Magn. Magn. Mater. Volume 59, Issues 3–4, pp. 351–356, 1986.

[35] S. Blundell, Magnetism in condensed matter, Oxford University Press Inc., New York, 2000.